

Super-twisting sliding mode control for brushless doubly-fed reluctance generator based on wind energy conversion system

Introduction. Recently, wind power generation has grown at an alarming rate in the past decade and will continue to do so as power electronic technology continues to advance. **Purpose.** Super-twisting sliding mode control for brushless doubly-fed reluctance generator based on wind energy conversion system. **Methods.** This paper deals with the robust power control of a grid-connected brushless doubly-fed reluctance generator driven by the variable speed wind turbine using a variable structure control theory called sliding mode control. The traditional sliding mode approach produces an unpleasant chattering phenomenon that could harm the system. To eliminate chattering, it is necessary to employ a high-order sliding mode controller. The super-twisting algorithm is one type of nonlinear control presented in order to ensure the effectiveness of the control structure we tested these controllers in two different ways reference tracking, and robustness. **Results.** Simulation results using MATLAB/Simulink have demonstrated the effectiveness and robustness of the super-twisting sliding mode controller. References 31, figures 14.

Key words: wind power, brushless doubly-fed reluctance generator, maximum power point tracking, vector control, super-twisting algorithm.

Вступ. В останнє десятиліття виробництво вітрової енергії зростало загрозливими темпами і продовжуватиме зростати у міру розвитку технологій силової електроніки. **Мета.** Управління ковзним режимом суперскручування для реактивного безщіткового генератора з подвійним живленням на основі системи перетворення енергії вітру. **Методи.** У цій статті розглядається надійне керування потужністю підключеного до мережі безщіткового реактивного генератора з подвійним живленням, що приводиться в дію вітряною турбіною зі змінною швидкістю, з використанням теорії управління зі змінною структурою, яка називається керуванням в ковзному режимі. Традиційний підхід зі ковзним режимом створює неприємне явище вібрації, що може зашкодити системі. Для усунення вібрації необхідно використовувати регулятор ковзного режиму високого порядку. Алгоритм суперскручування - це один із типів нелінійного управління, представлений для забезпечення ефективності структури управління. Ми протестували ці контролери двома різними способами: відстеженням посилення та надійністю. **Результати** моделювання з використанням MATLAB/Simulink продемонстрували ефективність та надійність контролера ковзного режиму суперскручування. Бібл. 31, рис. 14.

Ключові слова: енергія вітру, безколекторний реактивний генератор з подвійним живленням, відстеження точки максимальної потужності, векторне управління, алгоритм суперскручування.

Introduction. Researchers have long been looking for alternative form of energy production driven by the environmental concerns and the operational cost. This led to an increased study on renewable form of energy in recent years [1]. The first wind turbine (WT) was developed to generate electricity. Wind power was remarked as one of the promising renewable energy sources in the decade 1980-1990 [2]. The use of wind energy does not cause harmful emissions like greenhouse gases during its operating period and, without any surprise, worldwide wind power is one of the rapidly growing renewable energy sources. According to the World Wind Association, wind capacity over the world has reached up to 744 GW in 2020 [3], which was 318 MW in 2013 [4].

The brushless doubly-fed reluctance machine (BDFRM) has been investigated during the last decade as a potential alternative to the existing solutions in variable speed applications with narrow speed range [5]. The brushless doubly-fed induction machine (BDFIM) and the BDFRM are the two main competitors attracting most of the attention from researchers [6].

The following are the main benefits of BDFRM [7, 8]:

- maintenance free operation due to sturdy construction (no brushes or sliding rings) and great dependability, as opposed to the classic doubly-fed induction machine (DFIM);
- implicitly medium speed functioning enables the use of a two stage gearbox rather than a susceptible three stage equivalent with DFIMs, providing improved mechanical robustness and reduced failure rates, resulting in obvious cost savings;
- a lower capacity power electronics converter (about 25-30 % of the machine rated) for WTs and pump motors with a typical speed range of 2:1;

- operating mode flexibility as it can operate as a classical induction machine, or as a fixed/adjustable speed synchronous turbo machine, enabling high speed, field-weakened traction applications as well as high-frequency generators.

The brushless doubly-fed reluctance generator (BDFRG) has two three-phase windings in its stator: primary (or power) winding and secondary (or control) winding and have different pole pairs. So, a reluctance rotor, which the number of its salient poles is equal with sum of the primary and secondary pole pairs, provides coupling between the windings [9]. The primary winding is connected to the grid and the secondary to an inverter. These two windings always have different pole numbers [10]. Various control methodologies have been investigated for the BDFRM including: scalar control [11], vector control or field oriented control [12-14], control without a shaft position [15] or sensorless speed control [16] and direct power control [17]. These controllers are not robust against parameters variations, model uncertainties and external perturbations and are able to give an asymptotic convergence. Their main appeal is the rather low computational cost along with their simple implementation.

The linear control encountered difficulties since variable speed wind turbine (VSWT) system is a complex and highly non-linear system with strong coupling features and uncertainty in both the aerodynamic and the electrical parts. Thus, various non-linear control methods on VSWTs have been proposed, such as H_∞ control, robust control, feedback linearization technique, neural networks [18] control model reference adaptive system [19], model predictive [20], sliding mode control (SMC)

[14], synergetic-super-twisting algorithms [21], fuzzy model-based multivariable predictive regulator [22].

Apart from these non-linear controller, variable structure SMC has gained increased attention for the BDFRG-based wind energy conversion system (WECS) owing to its robust nature against both modeled and unmodeled external disturbance, fault scenarios, parameter variations, simple structure, low parameter sensitivity and easy implementation for wind extraction a number of SMC techniques have been proposed in the literature [23].

The traditional sliding mode approach produces an unpleasant chattering effect, which could be detrimental to the system. Thus, it is suitable to explore the use of second-order sliding mode algorithms which inherit all the properties of SMC and attenuates chattering or high frequency vibrations in controlled quantity thus reducing mechanical stresses in the system [24], in [14] the author compared between SMC and vector control of a BDFRG based on WECS.

Recently, nonlinear super-twisting sliding mode techniques have become an interesting option to be used in several kinds of systems. SMC guaranties the robustness and finite time convergence of a nonlinear system if the attractiveness condition is verified. Several works have been published using this technique, for example in [25].

The grid side converter (GSC) of the BDFRG is limited to proportional-integral (PI) control. The strategy of the BDFRG based on WECS control mainly consist two separate controls: a) stator side converter; b) grid side converter (GSC). In this paper, an active and reactive power of the stator of BDFRG is employed in a control winding side converter where its input is presented for the GSC; however, the GSC is managed by traditional PI based control strategy. The suggested control strategy is based on the famous, super complicated algorithm, this latter guarantees more reliable chatter free transient response of the BDFRG parameters in comparison to the traditional PI.

WECS modeling. WT model. The mechanical power extracted by the turbine from the wind is defined as [26]:

$$P_t = \frac{1}{2} \cdot \rho \cdot A \cdot C_p(\lambda) \cdot V^3, \quad (1)$$

where ρ is the air density; $A = \pi R^2$ is the rotor swept area; R is the turbine radius; C_p is the power coefficient; λ is the tip speed ratio; V is the wind speed.

The power coefficient C_p represents the aerodynamic efficiency of the WT. It is determined by the tip speed ratio λ and the blade pitch angle β . The tip speed ratio is expressed as:

$$\lambda = \frac{\Omega_t \cdot R}{V}, \quad (2)$$

where Ω_t is the turbine speed; β is the blade pitch angle.

For our example, the power coefficient C_p is

$$C_p(\lambda, \beta) = 0.5176 \cdot \left(\frac{116}{\lambda_x} - 0.4\beta - 5 \right) e^{-\lambda_x} + 0.0068\lambda, \quad (3)$$

where

$$\frac{1}{\lambda_x} = \frac{1}{\lambda + 0.08\beta} - \frac{0.035}{\beta^3 + 1}. \quad (4)$$

The C_p curve is shown in Fig. 1, from which there is an optimum λ at which the power coefficient C_p is maximal.

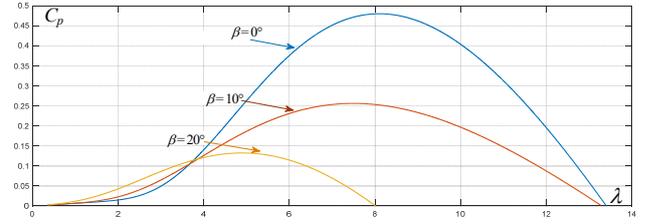


Fig. 1. Characteristics of the WT power coefficient with the tip speed ratio λ at different values of the blade pitch angle β

The maximum value of $C_p = 0.48$ is for $\beta = 0^\circ$ and for $\lambda = 8.1$.

The turbine torque can be written as:

$$T_t = P_t / \Omega_t. \quad (5)$$

The mechanical speed of the generator and the torque of the turbine referred to the generator are given by:

$$\begin{cases} \Omega_{mec} = \Omega_t \cdot G; \\ T_m = T_t / G, \end{cases} \quad (6)$$

where G is the gearbox ratio.

The mechanical equation of the system can be characterized by:

$$J \frac{d\Omega_{mec}}{dt} = T_m - T_{em} - f \cdot \Omega_{mec}, \quad (7)$$

where J is the equivalent total inertia of the generator shaft; f is the equivalent total friction coefficient; T_{em} is the electromagnetic torque.

To extract the maximum power from the WT, the electromagnetic torque command of the BDFRG, T_{e-ref} should be determined at the optimal value of the tip speed ratio and the corresponding maximum value of WT power coefficient C_p .

Mathematical model of BDFRG. The electrical equations of the BDFRG in the $d-q$ Park reference frame are given by:

$$\begin{cases} V_{pd} = R_p I_{pd} + \frac{d\Phi_{pd}}{dt} - \omega_p \cdot \Phi_{pq}; \\ V_{pq} = R_p I_{pq} + \frac{d\Phi_{pq}}{dt} + \omega \cdot \Phi_{pd}; \\ V_{sd} = R_s I_{sd} + \frac{d\Phi_{sd}}{dt} - (\omega_r - \omega) \cdot \Phi_{sq}; \\ V_{sq} = R_s I_{sq} + \frac{d\Phi_{sq}}{dt} + (\omega_r - \omega) \cdot \Phi_{sd}; \end{cases} \quad (8)$$

$$\begin{cases} \Phi_{pd} = L_p I_{pd} + L_m I_{sd}; \\ \Phi_{pq} = L_p I_{pq} - L_m I_{sq}; \\ \Phi_{sd} = L_s I_{sd} + L_m I_{pd}; \\ \Phi_{sq} = L_s I_{sq} - L_m I_{pq}. \end{cases} \quad (9)$$

The electromagnetic torque is expressed as:

$$T_e = \frac{3P_R L_m}{2L_p} (V_{pd} I_{sq} + V_{pq} I_{sd}). \quad (10)$$

The active and reactive powers equations at the primary stator, the secondary stator, and the grid are, respectively, written as:

$$\begin{cases} P_p = \frac{3}{2} (V_{pd} I_{pd} + V_{pq} I_{pq}); \\ Q_p = \frac{3}{2} (V_{pq} I_{pd} - V_{pd} I_{pq}); \end{cases} \quad (11)$$

$$\begin{cases} P_s = \frac{3}{2}(V_{sd}I_{sd} + V_{sq}I_{sq}) \\ Q_s = \frac{3}{2}(V_{sq}I_{sd} - V_{sd}I_{sq}) \end{cases} \quad (12)$$

$$\begin{cases} P_g = P_p + P_s; \\ Q_g = Q_p + Q_s, \end{cases} \quad (13)$$

where: V_{sd}, V_{sq} are the d-q axis control winding voltages; V_{pd}, V_{pq} are the d-q axis power winding voltages; R_p, R_s are the power and control winding resistances; L_p is the leakage inductance of power winding; L_s is the leakage inductance of control winding; L_m is the mutual inductance between power and control windings; I_{sd}, I_{sq} are the d-q axis control winding currents; I_{pd}, I_{pq} are the d-q axis power winding currents; ω_p is the angular frequencies of power windings; ω_s is the angular frequencies of control windings; ω_r is the BDFRG mechanical rotor angular speed; Φ_s is the d-q axis control winding flux linkages; Φ_p is the d-q axis power winding flux linkages.

GSC modeling and control. The grid-side converter maintains a constant DC-link voltage and satisfies the reactive power requirement in accordance with grid rules. Utilizing grid V_{OC} , active and reactive power may be easily regulated by d-axis and q-axis current. Two cascaded loops are used in this control approach. The inner loop controls grid current, while the outer loop controls DC-link voltage and reactive power for the GSC. The active power has a strong influence on the DC-link voltage [27].

The relationship between the grid and the converter are:

$$\begin{cases} L_f \frac{dI_{fd}}{dt} = -R_f I_{fd} + L_f \omega_s I_{fq} + V_{fd} - V_{sd}; \\ L_f \frac{dI_{fq}}{dt} = -R_f I_{fq} + L_f \omega_s I_{fd} + V_{fq} - V_{sq}. \end{cases} \quad (14)$$

As for the continuous side:

$$\frac{dV_{dc}}{dt} = \frac{1}{C}(I_s - I_l). \quad (15)$$

The forms of the grid active and reactive powers are as follow:

$$\begin{cases} P_s = \frac{3}{2}(V_{sd}I_{fd} + V_{sq}I_{fq}) \\ Q_s = \frac{3}{2}(V_{sq}I_{fd} - V_{sd}I_{fq}) \end{cases} \quad (16)$$

where V_{sd}, V_{sq} are the grid and converter voltage respectively; I_{fd}, I_{fq} are the grid and converter currents; R_f is the equivalent resistance of the grid filter; L_f is the inductance of the grid filter.

By orienting the inverter voltage on the grid side ($V_{sd} = 0$ and $V_{sq} = V$) we found:

$$\begin{cases} P_s = \frac{3}{2}V_{sq}I_{fq} = V_{dc}I_{dc}; \\ Q_s = \frac{3}{2}V_{sq}I_{fd}; \end{cases} \quad (17)$$

$$\begin{cases} V_{fd} = L_f \frac{dI_{fd}}{dt} + R_f I_{fd} - e'_q; \\ V_{fq} = L_f \frac{dI_{fq}}{dt} + R_f I_{fq} - e'_d; \end{cases} \quad \text{with} \quad \begin{cases} e_{fq} = -L_f \omega_s I_{fq}; \\ e_{fd} = -L_f \omega_s I_{fd} + V. \end{cases} \quad (18)$$

Figure 2 shows the block diagram of the control of the GSC.

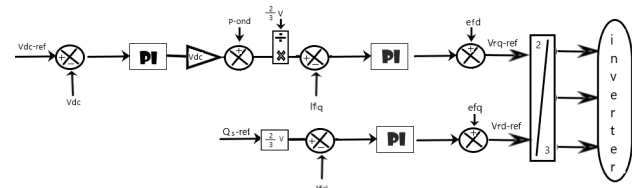


Fig. 2. Block diagram of grid side control

Vector control of the BDFRG. In order to decouple the stator active and reactive powers, the primary stator flux vector will be aligned with d -axis ϕ_{pd} ($\phi_{pd} = \phi_p$ and $\phi_{pq} = 0$), and the stator voltages will be expressed by:

$$\begin{cases} V_{pd} = 0; \\ V_{pq} = V_p = \omega_p \cdot \Phi_p. \end{cases} \quad (19)$$

The expressions of the primary stator currents are written as:

$$\begin{cases} I_{pd} = \frac{\Phi_{pd} - L_m I_{sd}}{L_p}; \\ I_{pq} = \frac{L_m I_{sq}}{L_p}. \end{cases} \quad (20)$$

By replacing these currents in the secondary stator fluxes equations, we obtain:

$$\begin{cases} \Phi_{sd} = L_s \sigma I_{sd} + \frac{L_m}{L_p} \Phi_{pd}; \\ \Phi_{sq} = \sigma L_s I_{sq}, \end{cases} \quad (21)$$

with σ is the leakage coefficient, defined by:

$$\sigma = 1 - \frac{L_m^2}{L_p L_s}. \quad (22)$$

The secondary stator voltages can be written according to the secondary stator currents as:

$$\begin{cases} V_{sd} = R_s I_{sd} + L_s \sigma \frac{dI_{sd}}{dt} + e_q; \\ V_{sq} = R_s I_{sq} + L_s \sigma \frac{dI_{sq}}{dt} + e_d + e_\phi, \end{cases} \quad (23)$$

with

$$\begin{cases} e_q = -\omega_s \sigma L_s I_{sq}; \\ e_d = \omega_s \sigma L_s I_{sd}; \\ e_\phi = \omega_s \frac{L_m}{L_p} \Phi_p, \end{cases} \quad (24)$$

the active and reactive stator powers of the BDFRG are expressed by:

$$\begin{cases} P_p = \frac{3V_{pq}L_m}{2L_p} I_{sq}; \\ Q_p = \frac{3}{2} \frac{V_{pq}^2}{\omega_p L_p} - \frac{3}{2} V_{pq} \frac{L_m}{L_p} I_{sd}, \end{cases} \quad (25)$$

where s is the slip of the BDFRG.

The electromagnetic torque can be written as:

$$T_e = \frac{3P_r L_m}{2L_p} I_{pd} I_{sq}. \quad (26)$$

For relatively weak sleep values and by neglecting the voltage drops, the grid active and reactive powers are simplified into:

$$\begin{cases} P_g = \frac{3(1-s)V_{pq}L_m}{2L_p} I_{sq}; \\ Q_g = \frac{3}{2} \frac{V_{pq}^2}{\omega_p L_p} - \frac{3(1-s)}{2} V_{pq} \frac{L_m}{L_p} I_{sd}. \end{cases} \quad (27)$$

From (27) we have:

$$\begin{cases} I_{sq} = \frac{2L_p}{3(1-s)V_{pq}L_m} P_g; \\ I_{sd} = \left(\frac{3V_{pq}^2}{2\omega_p L_p} - Q_g \right) \frac{2L_p}{3(1-s)V_{pq}L_m}. \end{cases} \quad (28)$$

Substitute (28) in (23) we obtain:

$$\begin{cases} \dot{P}_g = \frac{V_{sq}}{AL_s\sigma} - \frac{R_s}{L_s\sigma} P_g - \frac{ed}{AL_s\sigma} - \frac{e\varphi}{AL_s\sigma}; \\ \dot{Q}_g = \frac{-V_{sd}}{AL_s\sigma} - \frac{R_s}{L_s\sigma} Q_g + \frac{eq}{AL_s\sigma} + \frac{ev}{AL_s\sigma}, \end{cases} \quad (29)$$

with:

$$\begin{cases} A = \frac{2L_p}{3(1-s)V_{pq}L_m}; \\ ev = AR_s \frac{3V_{pq}^2}{2\omega_p L_p}. \end{cases} \quad (30)$$

In order to capture the optimal mechanical power, the control of the mechanical speed is applied as shown on Fig. 3.

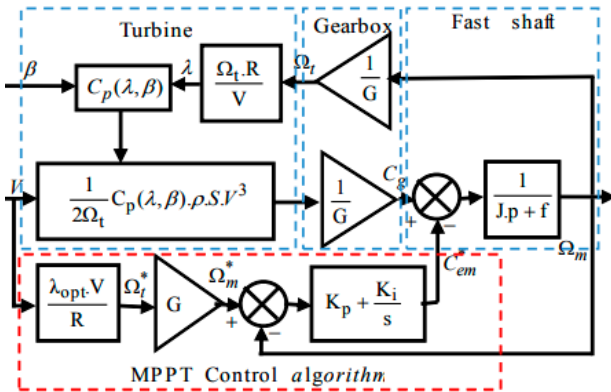


Fig. 3. MPPT with the control of the speed

The reference value of the active power exchanged between the wind generator and the grid is generated by maximum power point tracking (MPPT) control, and it's given by:

$$P_{g-ref} = T_{em-ref} \cdot \Omega_{mec}. \quad (31)$$

The reference grid reactive power, Q_{g-ref} is fixed to zero value to maintain the power factor at unity. The detailed scheme of the studied system is illustrated in Fig. 4 and presents a general schematic diagram of the BDFRG using super-twisting algorithm with GSC control.

High-order SMC. Control with high uncertainty is one of the most difficult control challenges. While there are a variety of advanced ways, such as adaptation based on identification and observation or perfect stability

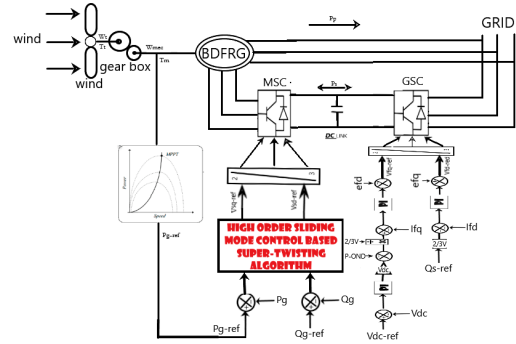


Fig. 4. The scheme of BDFRG using super-twisting algorithm with GSC control

techniques, the most apparent solution to engage with uncertainty is to «brutally enforce» some limitations. Therefore, any carefully maintained equality eliminates one «uncertainty dimension». The simplest technique to maintain a constraint is to respond instantly to any divergence of the system by stirring it back to the restriction with a suitably intense effort. When implemented directly, the method results in so-called sliding modes, which have become the primary operation modes in virtual switching system (VSS). They have demonstrated their great precision and resilience in the face of diverse internal and external disturbances [28].

The main drawbacks of the traditional SMC are chattering effect and discontinuous high-frequency switching control which is impractical. To overcome these problems, super-twisting controller is used. A single-dimensional motion of a unit mass system [29].

Second order SMC can only attenuate this problem. Twisting and super-twisting algorithms are the standard second order algorithms reported [25]. Today, the super-twisting method is preferred over the traditional sliding mode, since it eliminates the chattering phenomenon [24].

Super-twisting algorithm. To eliminate chattering in VSS, a super-twisting control method was proposed. It is a continuous controller which insures all the properties of the first order SMC for the system with matched bounded uncertainties/disturbances [30, 31].

For the dynamic system, the super-twisting control consists of two parts, a discontinuous part and a continuous part:

$$u = u_1 + u_2,$$

with

$$\begin{cases} u_1 = -\alpha |S|^\tau \text{sign}(S); \\ \dot{u}_2 = -\beta \text{sign}(S); \end{cases} \quad \tau \in 0,0.5; \quad (32)$$

where α, β checking for the following inequalities [24]:

$$\begin{cases} S(x,t) = \left(\frac{d}{dt} + \lambda \right)^{n-1} e; \\ \alpha^2 > \frac{4C_0 K_m (\alpha + C_0)}{K_m^3 (\alpha - C_0)}; \\ \beta > \frac{C_0}{K_m}, \end{cases} \quad (33)$$

where S is called the sliding surface; $x = [x, \dot{x}, \ddot{x}, \dots, x^{n-1}]$ is the state vector; $x^d = [x^d, \dot{x}^d, \ddot{x}^d, \dots, x^{d,n-1}]$ is the desired state vector; $e = x^d - x = [e, \dot{e}, \ddot{e}, \dots, e^{n-1}]$ is the error vector; λ is the positive coefficient; n is the system order; C_0, K_m are the positive constants.

High-order SMC of active and reactive powers.

The switching surfaces of the stator powers are given by:

$$\begin{cases} S(P_g) = e(P_g) = P_g - P_{g-ref}; \\ S(Q_g) = e(Q_g) = Q_g - Q_{g-ref}. \end{cases} \quad (34)$$

Then, we have:

$$\begin{cases} \dot{S}(P_g) = \dot{P}_g - \dot{P}_{g-ref}; \\ \dot{S}(Q_g) = \dot{Q}_g - \dot{Q}_{g-ref}. \end{cases} \quad (35)$$

From (29) we have:

$$\begin{cases} \dot{P}_g = \frac{V_{sq}}{AL_s\sigma} - \frac{R_s}{L_s\sigma} P_g - \frac{ed}{AL_s\sigma} - \frac{e\varphi}{AL_s\sigma}; \\ \dot{Q}_g = \frac{-V_{sd}}{AL_s\sigma} - \frac{R_s}{L_s\sigma} Q_g + \frac{eq}{AL_s\sigma} + \frac{ev}{AL_s\sigma}. \end{cases} \quad (36)$$

Now consider the following command:

$$\begin{cases} V_{sd} = u_2 + \alpha_1 |S(Q_g)|^\tau \text{sign}(S(Q_g)); \\ \dot{u}_2 = \beta_1 \text{sign}(S(Q_g)); \\ V_{sq} = w_2 + \alpha_2 |S(P_g)|^\tau \text{sign}(S(P_g)); \\ \dot{w}_2 = \beta_2 \text{sign}(S(P_g)); \\ \tau \in]0, 0.5[. \end{cases} \quad (37)$$

where the error $S(P)$ and $S(Q)$ are the sliding variables and constant gains α_1 , α_2 , β_1 , β_2 verify the stability conditions in (33).

Results and discussion. The control technique suggested in this paper has been approved by the MATLAB/Simulink software. The generator used in this simulation is 4.5 kW. This generator is connected directly to the grid through its primary stator and controlled through its secondary stator. Rated parameters [5] are: $R_p = 3.781 \Omega$; $R_s = 2.441 \Omega$; $L_p = 0.41 \text{ H}$; $L_s = 0.316 \text{ H}$; $L_m = 0.3 \text{ H}$; $J = 0.2 \text{ kg}\cdot\text{m}^2$; $P_r = 4$. WT parameters are: R (blade radius) = 4 m, gearbox ratio $G = 7.5$; turbine inertia $1.5 \text{ kg}\cdot\text{m}^2$, air density $\rho = 1.225 \text{ kg}/\text{m}^3$; number of blades = 3.

Figure 5 indicates the speed of the wind, and Fig. 6 – the generator speed. The mechanical speed generated by the turbine is similar to the wind profile applied to the turbine. The stator active power reference P_{g-ref} corresponding at its maximum is obtained by the WT with MPPT control. The reference value P_{g-ref} determined by (31), and the reference of the reactive power is maintained at zero to guarantee unity power factor.

The active and reactive powers follow perfectly and clearly their references with super-twisting algorithm without overshoot or dynamic errors.

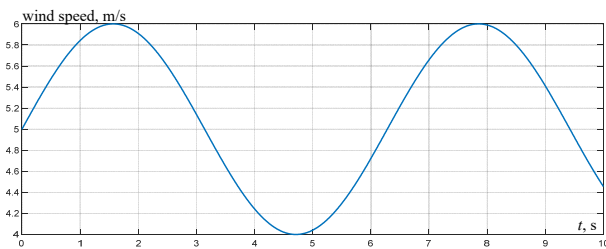


Fig. 5. Wind speed

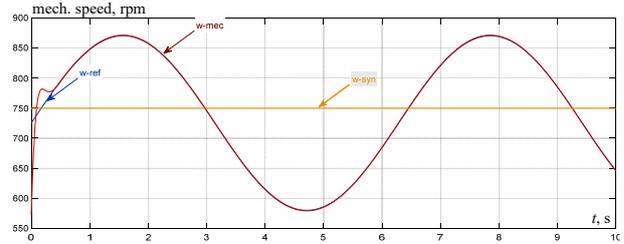


Fig. 6. Turbine mechanical speed

The simulation results illustrated in Fig. 7, 8 show the effectiveness of the control used for the control of the active and reactive powers, a good tracking is observed with a remarkable speed and precision. This chattering phenomenon is reduced with super-twisting controller [14].

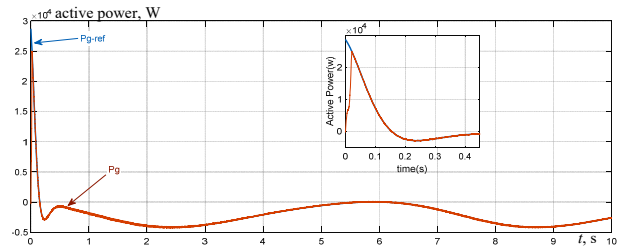


Fig. 7. Active power control

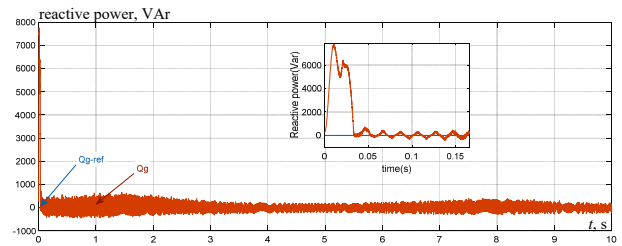


Fig. 8. Reactive power control

Figures 9, 10 present the winding currents in which we observe that both the frequency and the amplitude of these control currents (secondary currents I_s) change during the period of variation of active and reactive powers. Frequency of the current of the supply winding (primary currents I_p) remains constant to be adapted to the supply frequency of the grid, so when the reference of the active power is changed, the amplitude of the current also is changed.

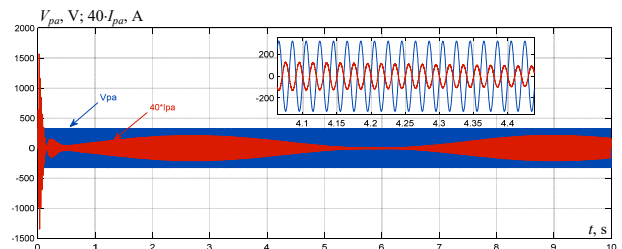


Fig. 9. Phase power winding current and voltage

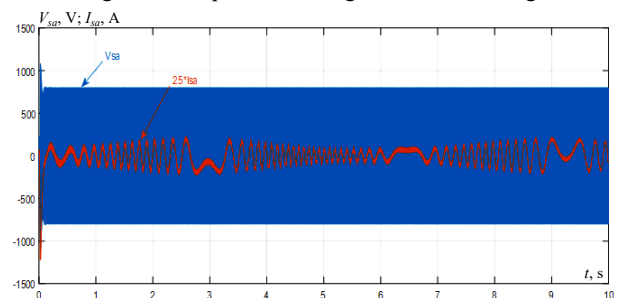


Fig. 10. Phase control winding current and voltage

Figure 11 demonstrates the voltage through the capacitor (direct voltage) throughout the shifting of power. It is clear that its pace follows well the reference (600 V).

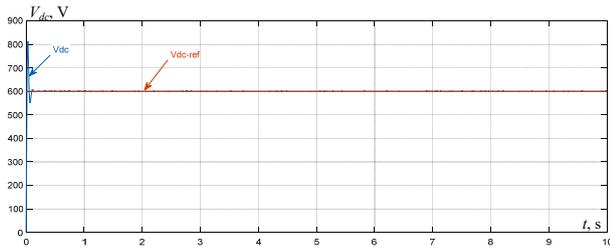


Fig. 11. DC bus voltage

Figure 12 demonstrates that the grid side reactive power follows her reference clearly on zero a good tracking so the unit power factor is ensured by the proposed controller.

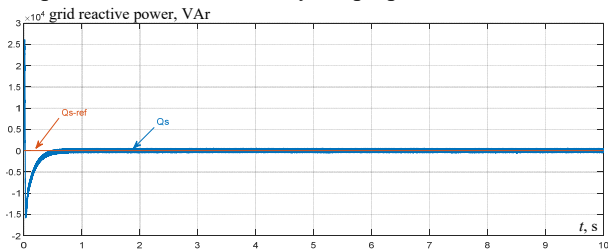


Fig. 12. Grid side reactive power control

Robustness test. The internal parameters of the BDFRG are dependent on variations caused by different physical parameters like temperature increase, saturation and skin effect, so our controller must provide good results against parameters variations of the generator.

In this test we have changed the values of the generator parameters (Fig. 13). Figure 14 demonstrates a tracking response of the reference value of the stator's active and reactive powers.

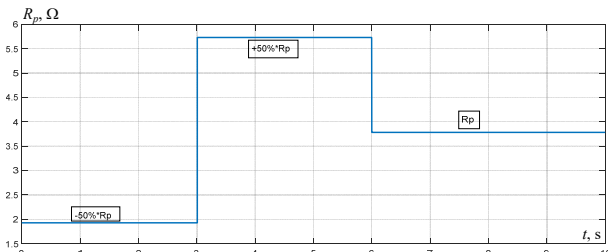


Fig. 13. Parameter variations (primary stator resistance variation)

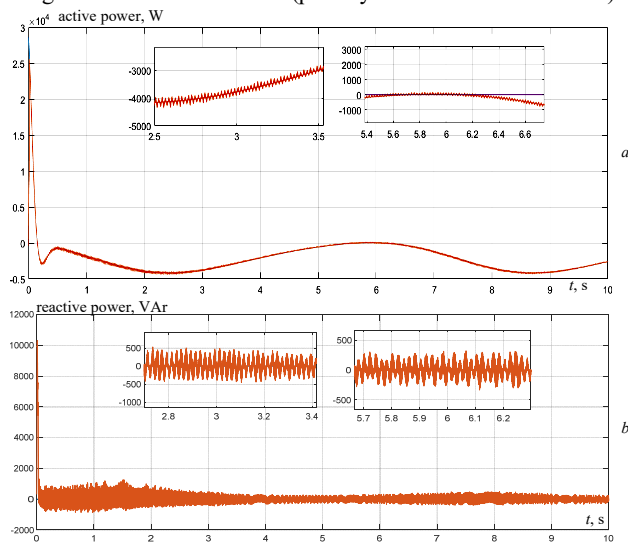


Fig. 14. Stator active and reactive power response

Conclusions. This paper has presented a super-twisting (second order sliding mode control) applied in wind energy system (variable speed wind turbine) to achieve the objectives of maximum power extraction and regulating the stator reactive power to follow grid requirements.

We have presented the wind turbine modeling and its maximum power point tracking control then we have provided the brushless doubly-fed reluctance generator modeling and its vector control. Super-twisting algorithm and its application to the brushless doubly-fed reluctance generator are described in order to ensure the effectiveness of the control structure we tested these controllers in two different ways reference tracking, and robustness.

Simulation results show the optimized performances of the super-twisting sliding mode controller. We observe high performances in terms of response time and reference tracking without overshoots through the response characteristics. The decoupling, the stability, and the convergence towards the equilibrium are assured. Furthermore, this regulation presents a high dynamic response, and it is more robust against parameter variation of the brushless doubly-fed reluctance generator.

Conflict of interest. The authors declare that they have no conflicts of interest.

REFERENCES

1. Fateh L., Ahmed O., Amar O., Abdelhak D., Lakhdar B. Modeling and control of a permanent magnet synchronous generator dedicated to standalone wind energy conversion system. *Frontiers in Energy*, 2016, vol. 10, no. 2, pp. 155-163. doi: <https://doi.org/10.1007/s11708-016-0410-1>.
2. Sami I., Ullah S., Ali Z., Ullah N., Ro J.-S. A Super Twisting Fractional Order Terminal Sliding Mode Control for DFIG-Based Wind Energy Conversion System. *Energies*, 2020, vol. 13, no. 9, art. no. 2158. doi: <https://doi.org/10.3390/en13092158>.
3. *Wind power capacity worldwide reaches 744 GW, 147 GW added in 2019*. Available at: <https://wwindea.org/information-2/statistics-news/> (Accessed 11 May 2022).
4. Ullah N., Asghar Ali M., Ibeas A., Herrera J. Adaptive Fractional Order Terminal Sliding Mode Control of a Doubly Fed Induction Generator-Based Wind Energy System. *IEEE Access*, 2017, vol. 5, pp. 21368-21381. doi: <https://doi.org/10.1109/ACCESS.2017.2759579>.
5. Ademi S., Jovanovic M. Vector control strategies for brushless doubly-fed reluctance wind generators. *2012 2nd International Symposium On Environment Friendly Energies And Applications*, 2012, pp. 44-49. doi: <https://doi.org/10.1109/EFEA.2012.6294084>.
6. Hopfensperger B., Atkinson D.J. Doubly-fed AC machines: classification and comparison. *European Power Electronics Conference*, 2001, vol. 200, no. 1.
7. Ademi S., Jovanovic M.G. Vector Control Methods for Brushless Doubly Fed Reluctance Machines. *IEEE Transactions on Industrial Electronics*, 2015, vol. 62, no. 1, pp. 96-104. doi: <https://doi.org/10.1109/TIE.2014.2327564>.
8. Jovanovic M. Sensorless and sensorless speed control methods for brushless doubly fed reluctance motors. *IET Electric Power Applications*, 2009, vol. 3, no. 6, pp. 503-513. doi: <https://doi.org/10.1049/iet-epa.2008.0227>.
9. Moazen M., Kazemzadeh R., Azizian M.-R. Mathematical proof of BDFRG model under unbalanced grid voltage condition. *Sustainable Energy, Grids and Networks*, 2020, vol. 21, art. no. 100327. doi: <https://doi.org/10.1016/j.segan.2020.100327>.
10. Betz R.E., Jovanovic M.G. Theoretical analysis of control properties for the brushless doubly fed reluctance machine. *IEEE Transactions on Energy Conversion*, 2002, vol. 17, no. 3, pp. 332-339. doi: <https://doi.org/10.1109/TEC.2002.801997>.

11. Jovanovic M. Control of Brushless Doubly-Fed Reluctance Motors. *Proceedings of the IEEE International Symposium on Industrial Electronics (ISIE 2005)*, 2005, pp. 1667-1672. doi: <https://doi.org/10.1109/ISIE.2005.1529182>.
12. Ademi S., Jovanovic M. Vector control strategies for brushless doubly-fed reluctance wind generators. *2012 2nd International Symposium On Environment Friendly Energies And Applications*, 2012, pp. 44-49. doi: <https://doi.org/10.1109/EFEA.2012.6294084>.
13. Ademi S., Jovanovic M.G., Hasan M. Control of Brushless Doubly-Fed Reluctance Generators for Wind Energy Conversion Systems. *IEEE Transactions on Energy Conversion*, 2015, vol. 30, no. 2, pp. 596-604. doi: <https://doi.org/10.1109/TEC.2014.2385472>.
14. Oualah O., Kerdoun D., Boumassata A. Comparative study between sliding mode control and the vector control of a brushless doubly fed reluctance generator based on wind energy conversion systems. *Electrical Engineering & Electromechanics*, 2022, no. 1, pp. 51-58. doi: <https://doi.org/10.20998/2074-272X.2022.1.07>.
15. Jovanovic M., Ademi S., Llano D.X. Control of Doubly-Fed Reluctance Machines without a Shaft Position or Speed Sensor. *2018 International Symposium on Power Electronics, Electrical Drives, Automation and Motion (SPEEDAM)*, 2018, pp. 1245-1250. doi: <https://doi.org/10.1109/SPEEDAM.2018.8445405>.
16. Kumar M., Das S., Sinha A.K. Sensorless speed control of brushless doubly-fed reluctance machine for pump storage and wind power application. *2018 IEEMA Engineer Infinite Conference (ETechNxt)*, 2018, pp. 1-6. doi: <https://doi.org/10.1109/ETECHNXT.2018.8385316>.
17. Zhu L., Zhang F., Jin S., Ademi S., Su X., Cao W. Optimized Power Error Comparison Strategy for Direct Power Control of the Open-Winding Brushless Doubly Fed Wind Power Generator. *IEEE Transactions on Sustainable Energy*, 2019, vol. 10, no. 4, pp. 2005-2014. doi: <https://doi.org/10.1109/TSTE.2018.2877439>.
18. Liu X., Han Y., Wang C. Second-order sliding mode control for power optimisation of DFIG-based variable speed wind turbine. *IET Renewable Power Generation*, 2017, vol. 11, no. 2, pp. 408-418. doi: <https://doi.org/10.1049/iet-rpg.2015.0403>.
19. Kiran K., Das S., Sahu A. Sensorless speed estimation and control of brushless doubly-fed reluctance machine drive using model reference adaptive system. *2016 IEEE International Conference on Power Electronics, Drives and Energy Systems (PEDES)*, 2016, pp. 1-6. doi: <https://doi.org/10.1109/PEDES.2016.7914480>.
20. Kiran K., Das S., Singh D. Model predictive field oriented speed control of brushless doubly-fed reluctance motor drive. *2018 International Conference on Power, Instrumentation, Control and Computing (PICC)*, 2018, pp. 1-6. doi: <https://doi.org/10.1109/PICC.2018.8384760>.
21. Benbouhenni H., Lemdani S. Combining synergetic control and super twisting algorithm to reduce the active power undulations of doubly fed induction generator for dual-rotor wind turbine system. *Electrical Engineering & Electromechanics*, 2021, no. 3, pp. 8-17. doi: <https://doi.org/10.20998/2074-272X.2021.3.02>.
22. Babes B., Hamouda N., Kahla S., Amar H., Ghoneim S.S.M. Fuzzy model based multivariable predictive control design for rapid and efficient speed-sensorless maximum power extraction of renewable wind generators. *Electrical Engineering & Electromechanics*, 2022, no. 3, pp. 51-62. doi: <https://doi.org/10.20998/2074-272X.2022.3.08>.
23. Oualah O., Kerdoun D., Boumassata A. Comparison between sliding mode and traditional PI controllers in a speed control of a brushless doubly fed reluctance machine. *1st International Conference on Scientific and Academic Research (ICSAR 2022)*, December 10-13, 2022, Konya, Turkey, pp. 1-6.
24. Boubzizi S., Abid H., El hajjaji A., Chaabane M. Comparative study of three types of controllers for DFIG in wind energy conversion system. *Protection and Control of Modern Power Systems*, 2018, vol. 3, no. 1, art. no. 21. doi: <https://doi.org/10.1186/s41601-018-0096-y>.
25. Kelkoul B., Boumediene A. Stability analysis and study between classical sliding mode control (SMC) and super twisting algorithm (STA) for doubly fed induction generator (DFIG) under wind turbine. *Energy*, 2021, vol. 214, art. no. 118871. doi: <https://doi.org/10.1016/j.energy.2020.118871>.
26. Boumassata A., Kerdoun D., Oualah O. Maximum power control of a wind generator with an energy storage system to fix the delivered power. *Electrical Engineering & Electromechanics*, 2022, no. 2, pp. 41-46. doi: <https://doi.org/10.20998/2074-272X.2022.2.07>.
27. Zhou D., Song Y., Blaabjerg F. Control of Wind Turbine System. In *Book: Control of Power Electronic Converters and Systems*, 2018, pp. 269-298. doi: <https://doi.org/10.1016/B978-0-12-805245-7.00010-X>.
28. Levant A. *Introduction to high-order sliding modes*. School of Mathematical Sciences, Israel, 2003. 55 p.
29. Durga Rao R. Implementation of fuzzy based power control of BDFIG with super-twisting sliding mode control. *JAC : A Journal of Composition Theory (JCT)*, 2020, vol. 13, no. 3, pp. 454-461.
30. Shiralkar A., Kurode S. Generalized super-twisting algorithm for control of electro-hydraulic servo system. *IFAC-PapersOnLine*, 2016, vol. 49, no. 1, pp. 742-747. doi: <https://doi.org/10.1016/j.ifacol.2016.03.145>.
31. Mahgoun M.S., Badoud A.E. New design and comparative study via two techniques for wind energy conversion system. *Electrical Engineering & Electromechanics*, 2021, no. 3, 18-24. doi: <https://doi.org/10.20998/2074-272X.2021.3.03>.

Received 25.08.2022
Accepted 06.12.2022
Published 07.03.2023

O. Oualah¹, PhD,
D. Kerdoun¹, Doctor of Electrotechnical, Professor,
A. Boumassata², Doctor of Electrotechnical,
¹ LGEC Research Laboratory,
Department of Electrical Engineering,
Brothers Mentouri University Constantine 1, Algeria,
e-mail: oussama.oulha@umc.edu.dz (Corresponding Author),
Kerdjallel@yahoo.fr
² National Polytechnic School Constantine, Algeria,
e-mail: a_boumassata@umc.edu.dz

How to cite this article:

Oualah O., Kerdoun D., Boumassata A. Super-twisting sliding mode control for brushless doubly fed reluctance generator based on wind energy conversion system. *Electrical Engineering & Electromechanics*, 2023, no. 2, pp. 86-92. doi: <https://doi.org/10.20998/2074-272X.2023.2.13>